J Therm Anal Calorim (2015) 121:1321–1332
DOI 10.1007/s10973-015-4554-8

Microstructure and non-isothermal crystallization behavior of PP/PLA/clay hybrid nanocomposites

Hassan Ebadi-Dehaghani · Mahdi Barikani · Hossein Ali Khonakdar · Seyed Hassan Jafari

Received: 3 January 2015 / Accepted: 8 February 2015 / Published online: 1 April 2015

Abstract Various compositions of polypropylene (PP) and poly(lactic acid) (PLA) blends were prepared by one-step melt compounding in a twin-screw extruder. Two compositions were selected for investigation of effect of clay and *n*-butyl acrylate glycidyl methacrylate ethylene terpolymer (PTW) as compatibilizer on thermal properties and non-isothermal crystallization behavior of PP/PLA/clay nanocomposite systems, i.e., PP-rich one (75/25 composition) containing Cloisite 15A and PLA-rich one (25/75 composition) containing Cloisite 30B. The thermal behavior of the systems was investigated by means of differential scanning calorimetry (DSC) and correlated with their microstructures. The narrowing down of the peaks in the wide-angle X-ray scattering pattern of PP-rich blend was associated with an increase in size and/or perfection of the crystals. On the other hand, the broadening of the peaks in PLA-rich blend implied a decrease in the size of the crystals. The calculated interlayer distance, using Scherrer equation, in Cloisite 15A was slightly greater than that of Cloisite 30B. Moreover, an increase of 100 % in interlayer distance showed a greater level of intercalation in PP-rich system as compared to the PLA-rich system. Blending of PP and PLA led to significant changes in the crystallinity behavior of the blends compared to the neat components. Moreover, the incorporation of the both clays into the two systems led to a greater change in the crystallinity degree, comparing to that of unfilled blends.

Keywords PP/PLA blends · Clay nanoparticles · Nanocomposites · Thermal properties · Microstructure

Introduction

Hybrid biocomposite systems with a multiphase polymeric matrix have attracted attention in recent years because the mechanical, physical, optical and rheological properties of a polymer blend can often be modified with incorporating a low content of inorganic nanofillers [1–3]. This attention is due to the fact that one or more components can be bio-based made from renewable sources. Interests in poly(lactic acid) (PLA) blend nanocomposites have emerged due to their biodegradability for use in packaging and engineering applications [2, 3]. Biodegradable films based on biopolymers have been developed, for important purposes, e.g., to control the gas permeability, preservation of surface integrity of products in the packaging industries. Modified atmosphere packaging (MAP) material issue is one of the interesting subjects of recent studies. Due to its polar structure, PLA is an engineering plastic with high oxygen barrier properties. Polypropylene (PP) is an excellent polymer with a combination of outstanding physical, chemical, mechanical, thermal and electrical properties. It is a commodity polymer in the packaging industries, but its poor barrier property to O_2 limits its applications [4]. Blending of PP and PLA can improve

H. Ebadi-Dehaghani · H. A. Khonakdar (✉)
Iran Polymer and Petrochemical Institute,
P.O. Box 14965/115, Tehran, Iran
e-mail: hakhonakdar@gmail.com

H. Ebadi-Dehaghani
e-mail: ebadi@iaush.ac.ir

M. Barikani · H. A. Khonakdar
Leibniz Institute of Polymer Research Dresden, 01067 Dresden, Germany

S. H. Jafari
School of Chemical Engineering, College of Engineering,
University of Tehran, P.O. Box 11155-4563, Tehran, Iran

barrier properties in the blend comparing to that for pure PP, due to lower oxygen permeability of PLA. Meanwhile, crystallization behavior is a significant factor, determining the diffusion of gases through a membrane [5]. The crystallinity degree is of great importance because the mass transport phenomena happen more easily in amorphous regions comparing to that of crystal lattices [5].

Commercial PLA is a mixture of D- and L-lactides. The L-isomer constitutes the main fraction of PLA derived from renewable sources since the majority of lactic acid from biological sources exists in this form. Depending on the composition of the optically active L- and D,L-enantiomers, PLA can crystallize in three forms (α, β and γ). The α-structure is more stable and has a melting temperature (T_m) of 185 °C compared to the β-structure, with a Tm of 175 °C [6]. The optical purity of PLA, i.e., the ratio of the two lactides, influences the thermal, barrier and mechanical properties, crystallinity and even the degradation characteristics [7–11]. PLA polymers with a high L-content tend to be crystalline while those with lower optical purity are amorphous [8]. Moreover, T_m, glass transition temperature (T_g) and crystallinity decrease with decreasing L-isomer content [8, 11].

Although PLA possesses many desirable properties, its crystallization rate is extremely slow in comparison with commercial thermoplastics and achieving high degree of crystallinity in PLA is difficult [12–14]. Similar to other semi-crystalline polymers, the crystallization behavior of PLA depends on both the nucleation activation energy and the mobility of chain segments. The most viable method to increase the overall crystallization rate is the blending of nucleating agent and plasticizers. The thermal behavior can be examined using differential scanning calorimetry (DSC) studies detecting multiphase transitions such as glass transition, cold crystallization and melting. Of these thermal properties, crystallization is the most important from both a scientific and commercial point of view, because many mechanical properties and biodegradability of PLA significantly depend on its crystallinity [12–14].

The injection molding grade PLA with a D-lactide content of 4 % purchased in semicrystalline form was reported by Tábi et al. [15] to become amorphous even at very low cooling rates (without the use of nucleating agents) while processing into a product, or mixing with natural fillers or fibers using melt mixing techniques such as extrusion. They reported on the changes in crystallinity during injection molding processing and its effect on the reprocessing.

In order to improve the crystallinity degree as well as the barrier properties of PLA, incorporation of proper fillers is an alternative, changing the thermal properties significantly [1–3, 12–14]. The crystalline properties of PLA nanocomposites were studied by Liang et al. [12] and Chow et al. [16] using DSC, to identify the influence of the nanometer particle content on the crystalline properties. Their results showed that thermal properties of PLA were greatly influenced by the addition of $CaCO_3$ [12] and organo-montmorillonite (OMMT) [16]. The crystallization onset temperature, crystallization temperature and crystallization end temperature as well as the crystalline degree of the composites in the presence of the nanoparticles were reported to be higher than those of the unfilled PLLA. The improvement of degree of crystallinity was attributed to the heterogeneous nucleation of the nano-$CaCO_3$ in the matrix [12].

Several works have been reported on the crystallization behavior of PLA hybrids [e.g., 3, 13–18]. The morphology, microstructure, thermal and rheological properties of PLA/polyhydroxybutyrate-valerate (PHBV) blends and PLA/PHBV/clay nanocomposites were investigated by Zhao et al. [13]. They reported on the effect of clay as a crystalline nucleating agent improving the crystallinity of the blends significantly, thus leading to a relatively high modulus for both solid and microcellular specimens.

According to the literature, the combined usage of PLA with PP seems to be a suitable choice for enhancing crystallization of PLA to improve barrier properties and incorporation of layered inorganic nanofiller, such as clay, enhances this phenomenon more and affects crystallization significantly [12, 16]. In our previous work, we reported on the effects of composition and compatibilization of PP/PLA blends on rheological properties of PP/PLA blends [19]. Considering the importance of crystallization phenomenon in PP/PLA/clay hybrid nanocomposite system having a multiphase crystallizable polymeric matrix and also influential role of clay and blend composition on this phenomenon, in the current study, we aim to investigate, for the first time, the effects of composition, clay inclusion and compatibilization process on crystallization and melting behavior of PP/PLA/clay hybrid nanocomposites. An attempt is also made to correlate the thermal properties with the microstructure of the developed systems and to study the nucleation ability of the clay nanoparticles in PP-rich and PLA-rich systems of this hybrid.

Experimental

Materials

Polypropylene (Moplen HP501H grade, MFI = 2.1 g per 10 min (230 °C/2.1 kg), density = 0.9 g cm^{-3} supplied by Basell Co.). PLA (4043D grade, density = 1.24 g cm^{-3} purchased from Nature Works, USA). EBAGMA, a terpolymer of ethylene, butyl acrylate (BA) and glycidyl methacrylate(GMA), commercially known as Elvaloy PTW (MFI = 12 g per 10 min (190 °C/2.16 kg), density = 0.94 g cm^{-3}) used as a reactive compatibilizer was

supplied by DuPont, USA. Cloisite 30B and Cloisite 15A were supplied by Southern Clay Products Inc., USA. Prior to melt compounding, the materials were dried for 4 h at 80 °C in a vacuum oven.

Material processing

PP/PLA blends were prepared according to the procedure was reported in [19]. Table 1 lists the compositions. As shown in Table 1a, five PP/PLA binary blends covering the whole composition range were compounded without compatibilizer. Two systems were selected for considering the effect of compatibilizer and clay nanoparticles, i.e., PP-rich system (PP/PLA 75/25) and PLA-rich system (PP/PLA 25/75), as shown in Table 1a, c, respectively. The Cloisite 30B was chosen for PLA-rich system due to the polar nature of PLA and better affinity between this nanoclay and PLA. A nonpolar organoclay Cloisite 15A with long alkyl tail surfactant was used for the PP-rich system [14].

Transmission electron microscopy (TEM)

The dispersion quality of the nanoparticles within the matrix and the nanostructures of the nanocomposites were investigated using a transmission electron microscope (TEM) on a Philips EM208 microscope (Netherlands), operated at 100 kV. The samples were microtomed at −160 °C.

Table 1 Composition of the samples (a) uncompatibilized blends, (b) PP-rich system and (c) PLA-rich system

Components	Composition
(a) Uncompatibilized blends	
Pure PP	100/0
PP/PLA	75/25
PP/PLA	50/50
PP/PLA	25/75
Pure PLA	0/100
(b) PP-rich system	
PP/PLA/PTW	75/25/5
PP/PLA/Cloisite 15A	75/25/3
PP/PLA/Cloisite 15A	75/25/5
PP/PLA/Cloisite 15A	75/25/7
PP/PLA/PTW/Cloisite 15A	75/25/5/5
(c) PLA-rich system	
PP/PLA/PTW	25/75/5
PP/PLA/Cloisite 30B	25/75/3
PP/PLA/Cloisite 30B	25/75/5
PP/PLA/Cloisite 30B	25/75/7
PP/PLA/PTW/Cloisite 30B	25/75/5/5

Scanning electron microscopy

Scanning electron microscopy (SEM) was used to characterize the morphology of cryofractured surface of the samples. The samples sputter coated with Pt prior to examination and observed under a NEON 40 EsB (Carl Zeiss, Oberkochen, Germany). SEM images were analyzed using image processing software (JMicroVision v1.27). The volume (R_v) and number (R_n) average radii and polydispersity of the particles (PD) were calculated using Eqs. 1–3 [19]. At least 200 particles were used to measure the parameters.

$$\bar{R}_n = \frac{\sum n_i R_i}{\sum n_i} \quad (1)$$

$$\bar{R}_V = \frac{\sum n_i R_i^4}{\sum n_i R_i^3} \quad (2)$$

$$PD = \frac{\bar{R}_V}{\bar{R}_n} \quad (3)$$

where n_i is the number of the droplets having radius R_i.

Differential scanning calorimetry (DSC)

A Mettler DSC (STARe SW 10.00) was used to study the crystallization degree of the specimens. Samples of two systems, i.e., PP-rich (75/25) and PLA-rich (25/75), were selected in order to investigate effect of composition, compatibilization and incorporation of clay nanoparticles on thermal properties. About 5 mg of each sample was scanned in a cycle of heating–cooling–heating from −20 to 200 °C. Thermal history was removed by scanning to 200 °C with a heating rate of 10 K min^{-1} and holding for 5 min. After cooling down, it was reheated with the same rate from room temperature to 200 °C to obtain the melting peaks.

In order to determine the crystallization enthalpy (ΔH_c), cold crystallization enthalpy (ΔH_{cc}) and melting enthalpy (ΔH_m), the cooling and second heating scans were used. The degree of crystallinity (X_c) of samples was calculated using the following equation [14]:

$$X_c = \frac{\Delta H}{\Delta H_m^0 \cdot [1 - (\text{mass\%. filler}/100)]} \times 100 \quad (4)$$

where $\Delta H = \Delta H_c$ for cooling curves, i.e., the crystallization enthalpy of the sample, or $\Delta H = \Delta H_m - \Delta H_{cc}$ for second heating curves, ΔH_m is the melting enthalpy of the sample, ΔH_{cc} is the cold crystallization enthalpy of the sample and ΔH_m^0 is the melting enthalpy of the 100 % crystalline polymer matrix (201.1 J g^{-1} for PP [20] and 93.0 J g^{-1} for PLA [18]) and mass% filler is the total mass percentage of nanoclay and blend component [21, 22].

Wide-angle X-ray scattering

Wide-angle X-ray scattering (WAXS) patterns were recorded using Cu Ka radiation ($\lambda = 1.54$ nm) generated by an X-ray diffractometer (Xpert, Philips) operated at 40 kV and 30 mA. The scanning rate was 1 min^{-1} with a step size of 0.1°.

Results and discussion

Morphology and microstructure

SEM, TEM, WAXS and DSC studies were carried out in order to investigate the relationship between the thermal properties and microstructures of the blends and nanocomposites. The SEM micrographs of the blends are shown in Fig. 1. The effects of compatibilization by the PTW and incorporation of nanocalay on the morphology of PP-rich and PLA-rich blends are shown in Fig. 2. These SEM images were elucidated using the image analyzer software. The Rn, Rv and PD values were calculated using Eqs. (1–3), and the results were reported in Table 2.

Comparing the micrographs of Fig. 1 shows that the discrete PLA spherical domains are almost uniformly dispersed in the matrices of the blends, but their sizes in the PLA-rich blend are greater than those of PP-rich one. Figure 2 shows the effects of compatibilization and incorporation of clay nanoparticles on the morphologies of PP-rich and PLA-rich blends. There is a decrease in the size of disperse phase and higher value of polydispersity of the droplet size with compatibilization using the PTW. This is corresponded to the effect of the PTW compatibilizer on the interfacial interaction between the phases, leading to reduce the droplet size and a greater polydispersity of them. Interestingly, with the introduction of 5 mass% Cloisite 15A and Cloisite 30B nanoparticles into the PP-rich and PLA-rich blends, respectively, the size of the dispersed domains decreases significantly (Fig. 2c, d).

Figure 3 shows the TEM microstructures of the nanocomposites. As shown, the clay nanoparticles in the non-compatibilized PP-rich and PLA-rich systems (Fig. 3a, c respectively) tend to be localized in the PLA phase. Compatibilization using the PTW compatibilizer for two systems changes the localization of the nanoparticles to the interphase region (Fig. 3b, d). Addition of compatibilizer to a clay-containing multiphase system can have its own contribution toward clay positioning and its state of dispersion due to induced changes in the system thermodynamic. This topic has been discussed intensively in the literature [3].

Another notable point is the degree of exfoliation/intercalation in the systems. A good compatibility between the clay and the organic polymer is an essential factor in order to achieve a proper dispersion of the individual silicate layers in a polymer matrix, known as an exfoliated morphology. However, in many cases, the silicate layers are not completely exfoliated and intercalation happens primarily. Therefore, both of the morphologies can be achieved. Comparing the TEM micrographs of Fig. 3a, b reveals that the extent of exfoliation of Cloisite 15A nanoparticles in the compatibilized PP-rich blend is greater

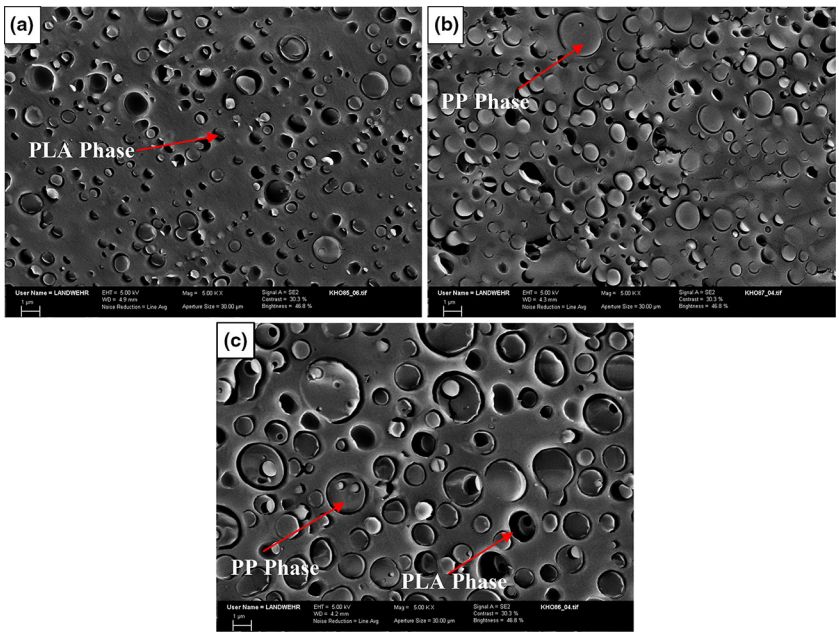

Fig. 1 Scanning electron micrographs of cryofractured surfaces of PP/PLA blends: **a** 75/25, **b** 25/75, **c** 50/50

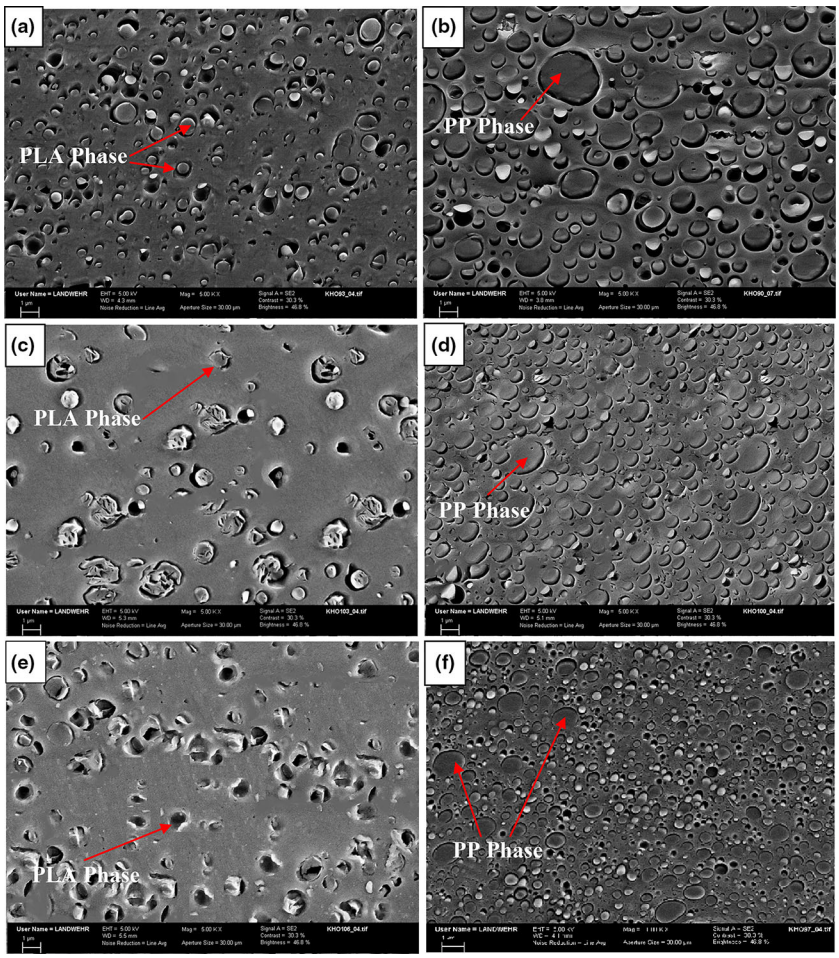

Fig. 2 Scanning electron micrographs of cryofractured surfaces of compatibilized blends and nanocomposites: **a** PP/PLA/PTW 75/25/5, **b** PP/PLA/PTW 25/75/5, **c** PP/PLA/Cloisite 15A 75/25/5, **d** PP/PLA/Cloisite 30B 25/75/5, **e** PP/PLA/Cloisite 15A/PTW 75/25/5/5, **f** PP/PLA/Cloisite 30B/PTW 25/75/5/5

than that for non-compatibilized one. Similarly, Fig. 3 shows that the exfoliation of Cloisite 30B in the PLA-rich system is greater in the presence of the PTW compatibilizer (Fig. 3d) as compare to non-compatibilized nanocomposite (Fig. 3c).

WAXS study

The morphological features of polymer nanocomposite, such as crystalline form and spherulite and nanoparticle size and also the nature of nanoparticles, can affect the final properties [23–25]. It is well known that PP mainly has three crystalline forms: monoclinic α, hexagonal β and orthorhombic γ. It has a para-crystalline smectic form too. However, β-PP is difficult to form unless specific nucleating agents are used [23, 24]. Figure 4a shows the WAXS patterns of pure PP, PLA and the blends. For the neat PP, the amorphous scattering is assumed to include that from the smectic phase. As shown in Fig. 4a, all of the samples, except for PLA, show five distinct α-form crystalline peaks at 2θ values of 14.0°, 16.8°, 18.5°, 21.8° and 21.9° [24], corresponding to 110, 040, 130, 111 and 041 reflections of the monoclinic α-crystalline phase of PP, respectively. However, the intensities of these peaks decrease with an increase in PLA content. The narrowing down of the peaks in PP-rich blend compared with those in the pure PP' WAXS pattern is associated with an increase in size and/or perfection of the crystals, as shown in Fig. 4a. Conversely, the broadening of the peaks in PLA-rich blend implies a decrease in the size of the crystals. The WAXS patterns of neat Cloisite 15A, and non-compatibilized PP-rich blends containing 0, 3, 5 and 7 mass% of Cloisite 15A are shown in Fig. 4b. Similarly, Fig. 4c shows the patterns for neat Cloisite 30B, and non-compatibilized PLA-rich blends containing 0, 3, 5 and 7 mass% of Cloisite 30B. Comparing the WAXS pattern of PP-rich blend and that of the nanocomposites shows an increase in crystallinity. In order to consider the effect of compatibilization, the WAXS

patterns of neat Cloisite 15A, and compatibilized and non-compatibilized PP-rich blends containing 5 mass% of Cloisite 15A are shown in Fig. 5a.

Assuming the width of the peaks to be solely due to the size, the d-spacing size of PP, blends and nanocomposites can be calculated by the Scherrer equation. The Scherrer formula is:

$$t = K\lambda/(B\cos\theta) \quad (5)$$

Table 2 Quantitative values obtained from SEM micrographs of the blends compatibilized with various amounts of PTW

Components	Composition	$\bar{R}_n/\mu m$	$\bar{R}_V/\mu m$	PD
PP/PLA	75/25	0.54	0.81	1.52
PP/PLA	50/50	0.82	1.22	1.49
PP/PLA	25/75	0.64	0.99	1.55
PP/PLA/PTW	75/25/5	0.28	0.69	2.45
PP/PLA/Cloisite 15A	75/25/5	0.40	0.84	2.08
PP/PLA/PTW/Cloisite 15A	75/25/5/5	0.23	0.43	1.31
PP/PLA/PTW	25/75/5	0.54	0.79	1.46
PP/PLA/Cloisite 30B	25/75/5	0.57	1.07	1.88
PP/PLA/PTW/Cloisite 30B	25/75/5/5	0.31	0.61	1.94

where t is the average dimension of crystallites normal to the plane of the reflection used; K is the Scherrer constant, a somewhat arbitrary value that falls in the range 0.87–1.0 (it is usually assumed to be 1); and B is the integral breadth of a reflection (in radians 2θ) located at 2θ. The Scherrer formula is only applicable if the particle size is $\sim$200 nm or less [25]. In order to calculate the dimensions of the crystallites, we used the peaks at 2θ values of 14.0° corresponding to 110 reflection for PP. In order to calculate the intergallery spacing (interlayer distance) in the clays, the peaks at 2θ values of 2.35° and 4.7° were used for Cloisite 15A and 30B, respectively, both corresponding to 100 reflection. The characteristic peak for the clay is that of the diffraction at (100), such peak interdistance is expressed by d100. Based on the diffraction peak of Cloisite 15A and Cloisite 30B in WAXS patterns (Fig. 4b, c), having different treatments, the interlayer distance values were calculated. Crystallite size of each nanocomposite was also calculated from the WAXS peak broadening. Following Scherrer equation, the interlayer distances were determined for Cloisite 15A and 30B clays as well as for their nanocomposites [26–29]. The calculated sizes in the nanocomposites are reported in Table 3.

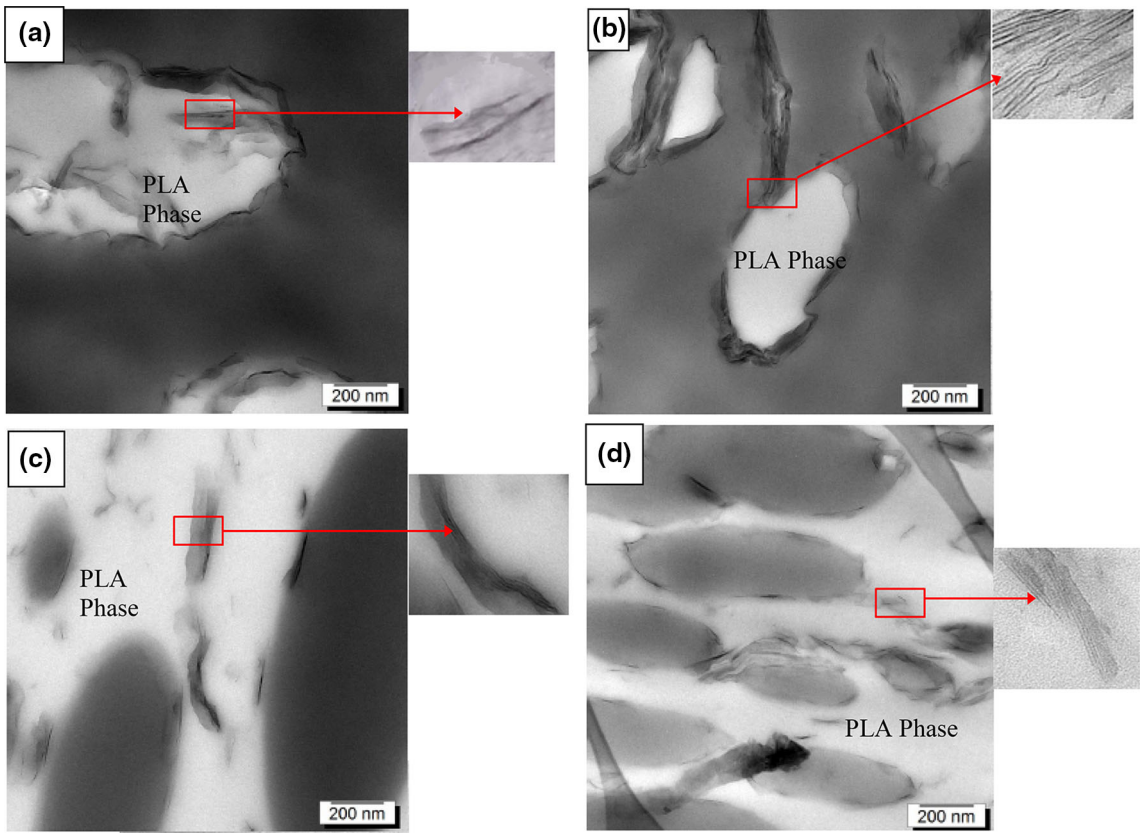

Fig. 3 Transmission electron micrographs of: **a** PP/PLA/Cloisite 15A 75/25/3, **b** PP/PLA/Cloisite 15A/PTW 75/25/5/5, **c** PP/PLA/Cloisite 30B 25/75/3, **d** PP/PLA/Cloisite 30B/PTW 25/75/5/5

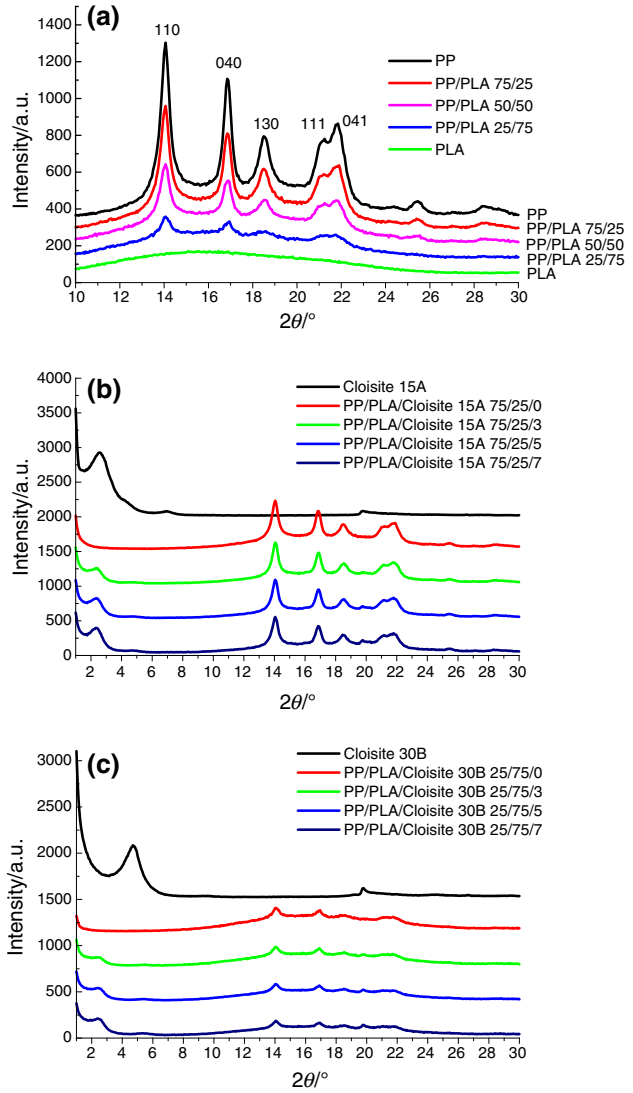

Fig. 4 WAXS patterns of **a** blend components and their blends, **b** neat Cloisite 15A and PP-rich nanocomposites, **c** neat Cloisite 30B and PLA-rich nanocomposites

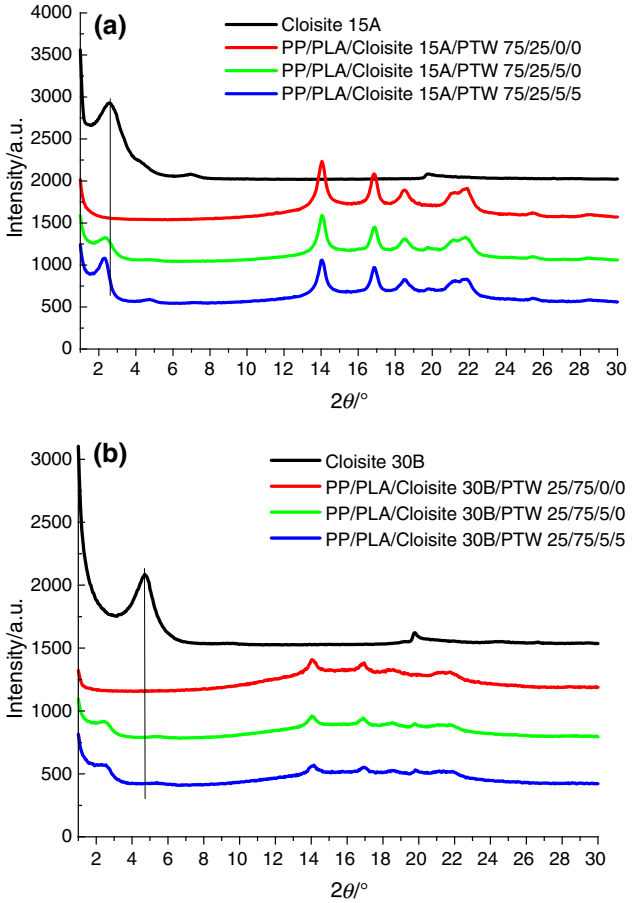

Fig. 5 WAXS patterns of neat nanoclays, unfilled blend, compatibilized and non-compatibilized blend nanocomposites of **a** PP-rich system, **b** PLA-rich system

Regarding to Fig. 4b, c and the calculated values shown in Table 3, the average dimensions of the crystallites increased with an increase in filler concentration in the both systems, corresponding to the nucleating effect of the nanofillers, causing crystallization at higher temperature.

Table 3 shows that the original interlayer distance in Cloisite 15A is slightly greater than that of Cloisite 30B. As shown in Fig. 5a and the data in Table 3, the characteristic peak of Cloisite 15A, at 2θ of 2.35°, has not been significantly shifted to the lower 2θ degree in PP-rich nanocomposites. However, an increase of 100 % in interlayer distance (Table 3) shows intercalated and exfoliated structure for them. Moreover, the height of this peak has decreased significantly in compatibilized nanocomposite, implying a structure with almost exfoliated tactoids.

Figure 5b shows the WAXS patterns of pure Cloisite 30B, and PLA-rich blend containing 5 mass% of Cloisite 30B without compatibilizer and that with compatibilizer. As clearly seen, the characteristic peak of Cloisite 30B, at 2θ of 4.7°, has been shifted significantly to a lower angle in the compatibilized and non-compatibilized PLA-rich blends. This shows presence of nanoparticles with intercalated structures in the nanocomposites. A comparison between interlayer distance values of Cloisites within PP-rich and PLA-rich blends with respect to that of neat ones (Table 3) shows that the interlayer distances of silicate layers within the PP-rich system are greater than that those of PLA-rich system. It can be due to different cationic modifiers present on the clay surfaces. Comparing to the cationic modifier of the Cloisite 30B surface, the modifier of Cloisite 15A has less affinity with PLA matrix due to the nonpolar nature of 15A and polar nature of PLA [14]. These results confirm that the structure of clay modifier is one of the most important factors that can influence the level of dispersion of nanoclays.

Table 3 Average dimensions of crystallites using Scherrer equation for diffractions of 110 and 100 for PP and Cloisites, respectively

Components	Composition	Peak position 2θ for 110 (PP)/°	Peak position 2θ for 100 (Cloisites)/°	B for 110 (PP)/°	B for 100 (Cloisites)/°	Crystallite sizes in PP/nm	Interlayer distance for Cloisites/nm
Pure PP	100/0	14	–	0.5	–	18.2	–
PP/PLA	75/25	14	–	0.46	–	19.8	–
PP/PLA	50/50	14	–	0.49	–	18.8	–
PP/PLA	25/75	14	–	0.55	–	16.7	–
PP/PLA/PTW	75/25/5	14	–	0.46	–	19.8	–
Cloisite 15A	–	–	2.3	–	0.84	–	10.6
PP/PLA/Cloisite 15A	75/25/5	14	2.3	0.45	0.45	16.7	19.6
PP/PLA/PTW/ Cloisite 15A	75/25/5/5	14	2.2	0.48	0.41	19.0	21.6
PP/PLA/PTW	25/75/5	14	–	0.5	–	18.2	–
Cloisite 30B	–	–	4.7	–	0.9	–	9.8
PP/PLA/Cloisite 30B	25/75/5	14	2.3	0.56	0.59	16.2	15.0
PP/PLA/PTW/ Cloisite 30B	25/75/5/5	14	2.2	0.43	0.62	21.2	14.2

Another notable point is that the addition of PTW compatibilizer to the composition can lead to a greater shift toward small angle and also decrease in the height of the peak implying a greater intercalation and exfoliation in the compatibilized PLA-rich blend. These results are in good agreement with the TEM images shown in Fig. 3 and confirm the microstructures explained therein.

Differential scanning calorimetry (DSC)

In this section, we investigate the effect of composition of the blends, and compatibilization using the PTW compatibilizer and addition of nanoclay and its content on the crystallization behavior of the two systems. The degree of crystallization (Xc) is used for comparison of the relative changes in the crystallization behavior. Figures 6, 7 and 8 represent the curves of all samples, and the obtained results are summarized in Table 4.

The curves of Fig. 6 show the effect of composition of the blends on the thermal properties of the blends. The second heating DSC analyses done from −20 to 180 °C show no glass transition and no cold crystallization temperature for PP in the investigated temperature range (Fig. 6a), but the endothermic peak of melting is at 164 °C. The DSC cooling curve of PP (Fig. 6b) shows one exothermic peak. This narrow exothermic peak with a maximum at 116 °C is the main peak due to the crystallization of PP. In the case of PLA, the second heating curve shows a glass transition at 60.7 °C. Moreover, there is a cold crystallization temperature at 121 °C, and the melting peak is at 152.7 °C. The DSC cooling curve for PLA is very smooth, and no exothermic peak can be observed, indicating that no crystallization occurs during the cooling process at this cooling rate (Fig. 6b). This suggests that melt crystallization of PLA is more difficult than cold crystallization in the non-isothermal quenching process.

Blending of PP and PLA leads to significant changes in the thermal behavior of the blends compared to pure components. As shown in Fig. 6a the second heating curve of the PP-rich blend shows an insignificant glass transition corresponding to the PLA phase, and a melting peak corresponding to the PP phase at 163.5 °C. The cooling DSC curve shows a narrow exothermic peak at 115.7 °C for this blend (Fig. 6b). This suggests a behavior for PP-rich blend similar to the PP. In the case of PLA-rich blend, there is a slight decrease in T_g and a significant decrease about 10 °C in cold crystallization temperature as compared to those for pure PLA. This decrease is attributed to a defective crystallization of PLA in the presence of PP droplets in the PLA-rich blend. The crystals in PLA-rich blend have been formed partially during cooling and partially during cold crystallization. This argument is confirmed by the shoulders in melting peak (Fig. 6a) and crystallization in cooling curve (Fig. 6b) and the data of Table 4. The effects of incorporation of the clay nanoparticles and compatibilization using the PTW compatibilizer on the thermal properties of PP-rich system are shown in Fig. 7. Regarding the second heating curves shown in Fig. 7a and transitions' values reported in Table 4, almost all of the samples in this system have not shown T_g transition except for non-compatibilized nanocomposite. Moreover, the unfilled blend that compatibilized using the PTW has not shown cold crystallization phenomenon. The incorporation of the Cloisite 15A clay has induced cold crystallization. Cold

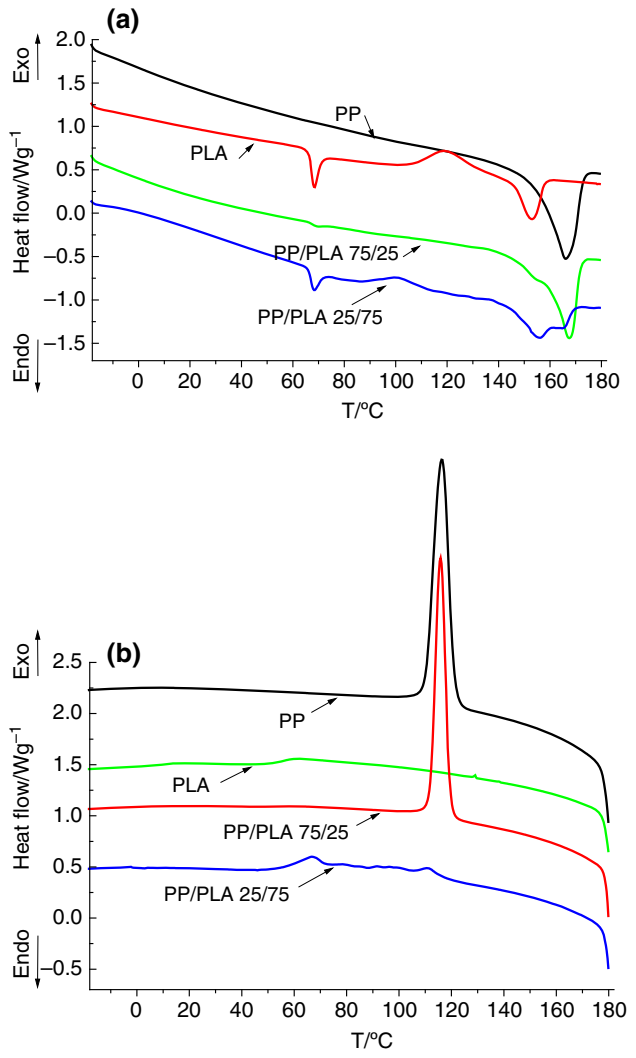

Fig. 6 DSC curves of the blend components; PP-rich and PLA-rich blends **a** second heating, **b** cooling

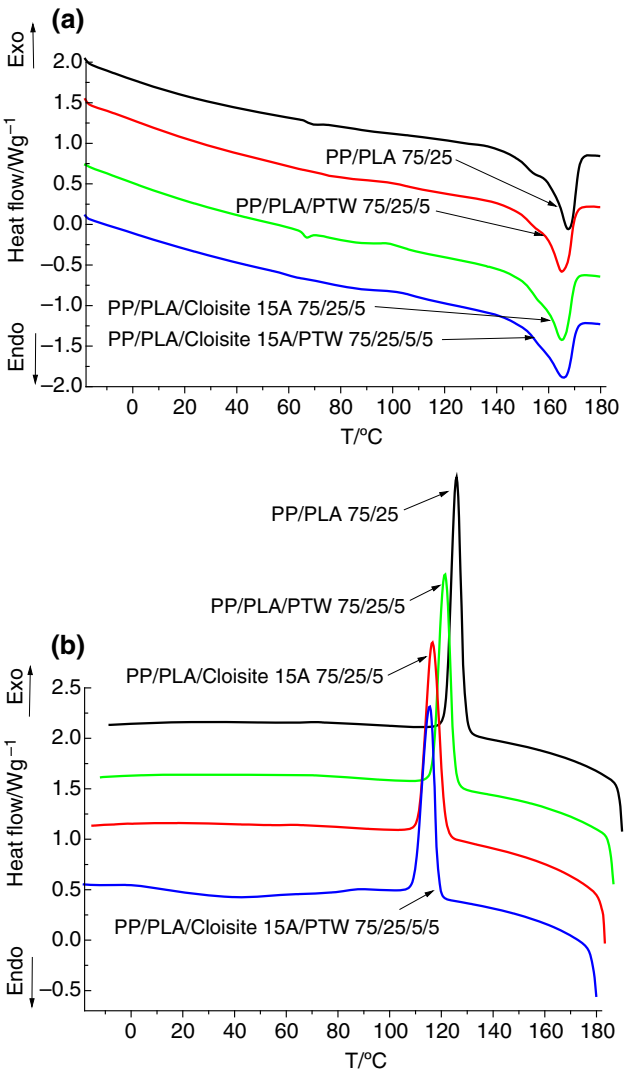

Fig. 7 DSC curves of the unfilled blend, compatibilized and non-compatibilized blend nanocomposites of the PP-rich system **a** second heating, **b** cooling

crystallization phenomena induced via nanoparticle incorporation were reported by other researchers [14, 30, 31]. This role of nucleating agent also is seen in the cooling DSC curve of Fig. 7b. This effect has been reflected in the Xc values (Table 4), as there is an increase in Xc value of PP-rich blend with incorporation of 5 mass% of Cloisite 15A.

The second heating DSC curves of the samples of PLA-rich system are shown in Fig. 8a. As shown, all of these samples show a T_g around 60 °C. There is a decrease in T_g value of PLA-rich sample with compatibilization using the PTW, implying that this is an effective compatibilizer for this system [33–35]. There is a decrease in T_{cc} value with incorporation of the Cloisite 30B nanoparticles to the PLA-rich blend with the help of the reported values in Table 4. In the PLA-rich system, the compatibilization using the PTW compatibilizer has reverse effect in the cold crystallization temperature. The results show that the addition of PTW leads to reduction in the crystallization process and crystallite formation, which subsequently reduce the degree of crystallinity of PP/PLA/clay nanocomposites. It is suggested that the nucleating efficiency maybe disappeared due to the compatibilizer action which encapsulates the nanoparticles, causing the kinetic restriction on the crystallization phenomenon. There are several works reported on the effect of interfacial interactions on the crystallization behavior of blends and nanocomposites [32–34]. For example, it was reported that the addition of acrylic acid-grafted polypropylene as compatibilizer improved the nucleation of CaCO3 nanoparticles in PP/CaCO3 nanocomposites, and the crystallization temperature of the composites increased because of the enhanced nucleation of the nanoparticles [33]. Yang et al.

[34] reported that addition of PP-g-MA and POE-g-MA into β-nucleated iPP/PA66 blends increased the β-crystal content of PP. Moreover, they reported that the increase in the non-isothermal crystallization temperature depends on the type of compatibilizer [34].

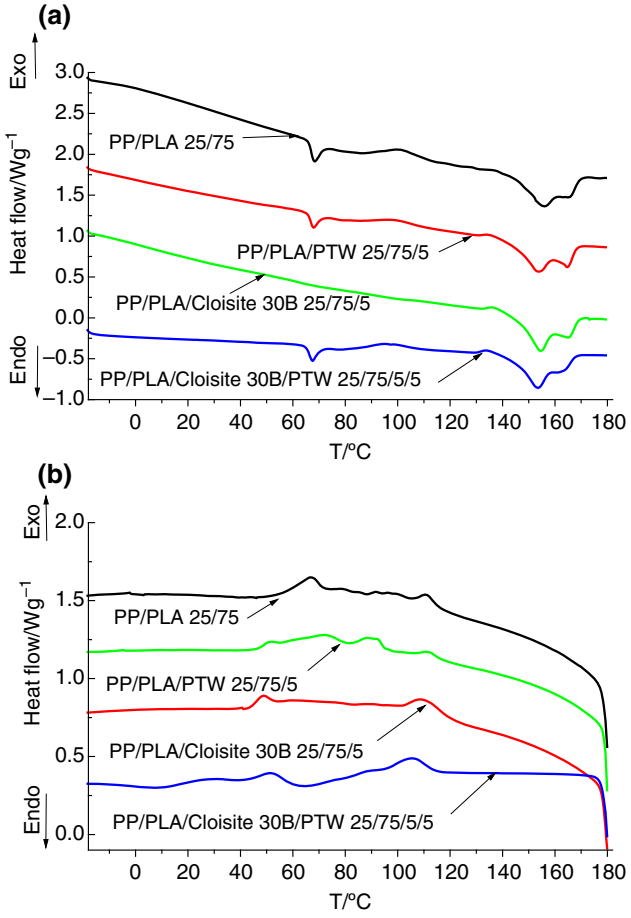

Fig. 8 DSC curves of the unfilled blend, compatibilized and non-compatibilized blend nanocomposites of the PLA-rich system **a** second heating, **b** cooling

It is acquired for a good nucleating agent that T_{cc} is decreased and Tc is increased [35–38]. Hence, the Cloisite 30B is a nucleating agent for PLA, while PTW is not a proper nucleating agent for it. A shoulder endothermic peak at approximately 154 °C was observed for PP-rich and PLA-rich samples; however, no similar peak was revealed for pure PLA. According to Martin and Avérous [35], a very small melting endotherm at 152 °C has been recorded and corresponded to the residual crystallinity. They also reported that these two distinct peaks are owing to the lamellar re-arrangement during crystallization of PLA. Di Lorenzo et al. [36] have reported that poly(Llactic acid) (PLLA) is a polymorph material that presents several crystal modification. A shoulder or low-temperature peak was reported to form on the melting endotherm of the original crystallites [37]. Scheirs [38] reported that multiple melting peaks can be observed in a number of semicrystalline polymers during a DSC scan. These occur when imperfect crystals that have melted at a lower temperature, recrystallize to give crystals at a higher temperature [16].

Figure 8b shows the cooling DSC curves of the PLA-rich samples. As shown, there are shoulders for all of the samples in this system resulting in complexity in analyzing the data. In other words, a fractionated crystallization of samples occurred during cooling. Such behaviors were also reported for PLA/LLDPE blends [14]. The crystallization of the minor component in incompatible polymer blends starts sometimes at distinctly larger undercooling than that of meat polymer, and proceeds in several separated steps. The most likely explanation for the appearance of several different exotherms in the molten PLA-rich blend is the fact that when the polymer is dispersed into droplets, the content of heterogeneities of each droplet could be different and also the polymer may contain different types of heterogeneities which will be activated at cooling depending on their specific interfacial energy differences with the molten polymer. When the polymer is in the bulk, the

Table 4 DSC analysis of the blend components and their nanocomposites at cooling/heating rate of 10 Kmin − 1

Sampled	Second heating							Cooling		
	T_g/°C	T_{cc}/°C	ΔH_{cc}/J g^{-1}	X_{cc}/%	T_m/°C	ΔH_m/J g^{-1}	X_m/%	T_c/°C	ΔH_c/J g^{-1}	X_c/%
Pure PP	–	–	–	–	164.2	101.9	51.0	116.4	100.5	50.0
PP/PLA 75/25	–	–	–	–	163.5	88.3	58.5	115.7	71.6	47.0
PP/PLA/PTW 75/25/5	–	–	–	–	162.7	77.3	51.2	114.7	66.1	44.0
PP/PLA/15A 75/25/5	60.5	107.2	5.5	3.9	162.7	67.2	47.7	113.3	68.6	48.7
PP/PLA/PTW/15A 75/25/5/5	–	112.3	5.9	4.5	163.2	62.6	47.9	115.3	62.5	47.8
Pure PLA	60.7	121.1	15.5	16.7	152.7	26.7	28.7	128.7	7.5	8.1
PP/PLA 25/75	61.5	109.9	15.3	21.9	154.7/163.4	1.3/39.3	2.5/56.3	91.6	0.5	1.0
PP/PLA/PTW 25/75/5	60.3	114.1	15.7	22.1	149.7/162.9	1.2/38.1	1.9/58.5	89.1	20.5	31.5
PP/PLA/30B 25/75/5	61.2	107.6	16.0	22.5	155.6/162.9	5.6/39.3	9.3/60.4	110.1	6.6	10.9
PP/PLA/PTW/30B 25/75/5/5	60.3	118.0	18.8	31.1	151.8	34.7	57.4	104.9	10.8	17.9

heterogeneity with the lowest specific interfacial energy difference is activated and dominates the crystallization of the polymer via secondary nucleation at the created crystals [39].

The data shown in Table 4 reveal that there is an increase in T_c and X_c of PLA with compatibilization using the PTW. Interestingly, incorporation of the Cloisite 30B nanoparticles has opposite effect on crystallization. This effect was also seen in the crystallite size that the size of crystals in non-compatibilized PLA-rich nanocomposite was smaller than that for unfilled PLA-rich one (Table 3).

The crystallization behavior of these systems and its influence on the mechanical properties was reported elsewhere [40]. There was an increase in Young's modulus with increase in degree of crystallinity. The results of experimental permeability values accompanied by a molecular dynamic simulation (MD) on diffusion of oxygen were also submitted elsewhere. The results of permeability values also agree with the results of crystallinity. The increase in crystallinity led to increase in barrier properties of the final hybrids.

Conclusions

The non-isothermal crystallization behaviors of PP, PLA and their blends and hybrid nanocomposites were investigated and correlated with the microstructure. Morphological studies were performed on PP/PLA blends with different compositions, i.e., PP-rich and PLA-rich ones containing different types of nanoclays, i.e., Cloisite 15A and 30B, respectively. It is found that the morphologies of the both systems being droplet in matrix were refined by addition nanoclays. The WAXS patterns of all the PP-containing samples showed five distinct crystalline peaks, corresponding to the monoclinic α-crystalline phase of PP. The narrowing down of the peaks in the WAXS pattern of PP-rich blend compared with those in the pure PP was associated with an increase in size and/or perfection of the crystals. Conversely, the broadening of the peaks in PLA-rich blend implied a decrease in the size of the crystals. Comparing the WAXS patterns of PP-rich and those of the nanocomposites showed an increase in degree of crystallinity. Moreover, the calculated values obtained by the Scherrer equation showed that the average dimensions of the crystallites increased with an increase in filler content in the both systems. This was attributed to the nucleating effect of the nanofillers, resulting in crystallization to occur at higher temperature.

The DSC results showed that for the neat PLA the melt crystallization in the non-isothermal quenching process was more difficult than cold crystallization. Blending of PP and PLA led to significant changes in the thermal behavior of the blends compared to pure components. While the thermal behavior of PP-rich blend was almost similar to the pure PP, there was a slight decrease in T_g and a significant decrease about 10 °C in the cold crystallization temperature in the case of PLA-rich blend, as compared to those for pure PLA. This decrease was attributed to an effective crystallization of PLA in the presence of PP droplets in the PLA-rich blend. There was a decrease in T_g value of PLA-rich sample with compatibilization using the PTW, implying that this was an effective compatibilizer for this system. While there was a decrease in T_{cc} value of PLA-rich sample with incorporation of Cloisite 30B, implying this clay is a good of nucleating agent for crystallization in PLA-rich blends. The study of crystallization behavior revealed that the Cloisite 15A clay, as a strong nucleating agent, altered the PP-rich blend crystallization during heating. In addition, the PLA crystals in PLA-rich system were formed during heating and fractionated crystallization of samples occurred during cooling. From the above results, it is concluded that regarding to the greater values of degree of crystallinity in the PP-rich system comparing to that for the PLA-rich one, resulting in high barrier properties, the PP-rich system can be used as a potential biodegradable material for modified atmosphere packaging (MAP).

Acknowledgements The work described in this paper was supported by a grant from the Iran Polymer and Petrochemical Institute (IPPI). The authors gratefully acknowledge the Research Vice Chancellor of IPPI and his co-workers for their helps and assistances.

References

1. Kim K-W, Lee B-H, Kim H-J, Sriroth K, Dorgan JR. Thermal and mechanical properties of cassava and pineapple flours-filled PLA bio-composites. J Therm Anal Calorim. 2012;108(3):1131–9.
2. Shi N, Dou Q. Non-isothermal cold crystallization kinetics of poly(lactic acid)/poly(butylene adipate-co-terephthalate)/treated calcium carbonate composites. J Therm Anal Calorim. 2014;. doi:10.1007/s10973-014-4162-z.
3. Tábi T, Suplicz A, Czigány T, Kovács JG. Thermal and mechanical analysis of injection moulded poly(lactic acid) filled with poly(ethylene glycol) and talc. J Therm Anal Calorim. 2014;118:1419–30.
4. Parry RT. Principle and applications of modified atmosphere packaging of food. New York: Chapman & Hall; 1993.
5. Vieth WR. Diffusion in and through polymers: principles and applications, Chapter 4. New York: Oxford University Press; 1991.
6. Auras R, Harte B, Selke S. An overview of polylactides as packaging materials. Macromol Biosci. 2004;4:835–64.
7. Sarasua JR, Arraiza AL, Balerdi P, Maiza I. Crystallinity and mechanical properties of optically pure polylactides and their blends. Polym Eng Sci. 2005;45:745–53.
8. Tsuji H, Ikada Y. Crystallization from the melt of PLA with different optical purities and their blends. Macromol Chem Phys. 1996;197:3483–99.

9. Hutchinson M, Dorgan J, Knauss D, Hait S. Optical properties of polylactides. J Polym Environ. 2006;14:119–24.
10. Pyda M, Bopp RC, Wunderlich B. Heat capacity of poly(lactic acid). J Chem Thermodynam. 2004;36:731–42.
11. Dorgan JR, Jansen J, Clayton MP. Melt rheology of variable l-content poly(lactic acid). J Rheol. 2005;49:607–19.
12. Liang J-Z, Zhou L, Tang C-Y, Tsui C-P. Crystalline properties of poly(L-lactic acid) composites filled with nanometer calcium carbonate. Compos B-Eng. 2013;45:1646–50.
13. Zhao H, Cui Z, Wang X, Turng L-S, Peng X. Processing and characterization of solid and microcellular poly(lactic acid)/polyhydroxybutyrate-valerate (PLA/PHBV) blends and PLA/PHBV/clay nanocomposites. Compos B-Eng. 2013;51:79–91.
14. As'habi L, Jafari S H, Khonakdar H A, Häussler L, Wagenknecht U, Heinrich G, Non-isothermal crystallization behavior of PLA/LLDPE/nanoclay hybrid: Synergistic role of LLDPE and clay, Thermochim Acta. 2013;565:102–13.
15. Tábi T, Sajó IE, Szaból F, Luyt AS, Kovács JG. Crystalline structure of annealed polylactic acid and its relation to processing, eXP. Polym Let. 2010;4(10):659–68.
16. Chow WS, Lok SK. Thermal properties of poly(lactic acid)/organo-montmorillonite nanocomposites. J Therm Anal Calorim. 2009;95(2):627–32.
17. Tsuji H, Tezuka Y. Stereocomplex formation between enantiomeric poly(lactic acid)s. 12. Spherulite growth of low-molecular-weight poly(lactic acid)s from the melt, Biomacromol. 2004;5:1181–6.
18. Rodrigues JAFR, Parra DF, Lugáo AB. Crystallization on films of PHB/PEG blends. J Therm Anal Calorim. 2005;79:379–81.
19. Ebadi-Dehaghani H, Barikani M, Khonakdar HA, Jafari SH, Wagenknecht U, Heinrich G. An investigation on compatibilization threshold in the interface of PP/PLA blends using rheological studies. J Vin Add Tech. 2014;. doi:10.1002/vnl.21424.
20. Bai F, Li F, Calhoun B, Quirk RP, Cheng SZD. Polymer Handbook. 4th ed. New York: John Wiley & Sons Inc.; 1999.
21. Brandrup J, Immergut EH. Polymer Hand Book. New York: Wiley; 1975.
22. Battegazzore D, Bocchini S, Frache A. Crystallization kinetics of poly(lactic acid)-talc composites. eXP Polym Let. 2011;5:849–58.
23. Labour T, Vigier G, Séguéla R, Gauthier C, Orange G, Bomal Y. Influence of the β-crystalline phase on the mechanical properties of unfilled and calcium carbonate-filled polypropylene: Ductile cracking and impact behavior. J Polym. Sci Part B-Polym Phys. 2002;40:31–42.
24. Qian J, Cheng G, Zhang H, Liu YX. Preparation and characterization of polypropylene/silica nanocomposites by gamma irradiation via ultrafine blend J Polym Res. 2011;18:409–17.
25. Scherrer P. Bestimmung der Größe und der inneren Struktur von Kolloidteilchen mittels Röntgenstrahlen. Nachrichten von der Gesellschaft der Wissenschaften zu Göttingen. 1918;2:98.
26. Bertoluzza A, Fagnano C. Morelli MA, Gotfardi V, Guglielmi M. Raman and Infra-Red spectra on silica gel evolving towards glass, J Non-Crystal Sol. 1982;48:1–17.
27. Ramez A, Occurrence M. Mineralogy of a deposit of Shampoo-clay in southern Iran. Appl Clay Sci. 1996;11:43–5.
28. Bahari A, Morgen P, Li ZS. Ultra-thin silicon nitride films on Si 100 studied with core level photoemission. Surf Sci. 2008;602:2315–24.
29. Hernandez-Torres J, Mendoza-Galvan A. Formation of NiO–SiO2 nanocomposite thin films by the sol–gel method. J. Nan crystalline solids. 2005;351:2029–35.
30. Fortunati E, Armentano I, Zhou Q, Puglia D, Terenzi A, Berglund LA, Kenny JM. Microstructure and nonisothermal cold crystallization of PLA composites based on silver nanoparticles and nanocrystalline cellulose. Polym Deg Stab. 2012;97:2027–36.
31. Lee SJ, Hahm WG, Kikutani T, Kim BC. Effects of clay and POSS nanoparticles on the quiescent and shear-induced crystallization behavior of high molecular weight poly(ethylene terephthalate). Polym Eng Sci. 2009;49:317–23.
32. Wan W, Yu D, Xie Y, Guo X, Zhou W, Cao J. Effects of nanoparticle treatment on the crystallization behavior and mechanical properties of polypropylene/calcium carbonate nanocomposites. J Appl Polym Sci. 2006;102:3480–8.
33. Lin ZD, Huang ZZ, Zhang Y, Mai KC, Zeng HM. Crystallization and melting behavior of nano-CaCO3/polypropylene composites modified by acrylic acid. J Appl Polym Sci. 2004;91:2443–53.
34. Yang Z, Mai K. Nonisothermal crystallization and melting behavior of β-nucleated isotactic polypropylene and polyamide 66 blends. J Appl Polym Sci. 2011;119:3566–73.
35. Martin O, Avérous L. Poly(lactic acid): plasticization and properties of biodegradable multiphase systems. Polymer. 2001;42:6209–19.
36. Di Lorenzo ML. Crystallization behavior of poly(L-lactic acid). Eur Polym J. 2005;41:569–75.
37. Yew G H, Mohd Yusof A M, Mohd Ishak Z A, Ishiaku U S. Water absorption and enzymatic degradation of poly(lactic acid)/rice starch composites, Polym Deg Stab. 2005;90:488-500.
38. Scheirs J. Compositional and Failure Analysis of Polymers: A Practical Approach. New York: John Wiley and Sons; 2000. p. 1.
39. Arnal ML, Matos ME, Morales RA, Santana OO, Müller AJ. Evaluation of the fractionated crystallization of dispersed polyolefins in a polystyrene matrix. Macromol Chem Phys. 1998;199:2275–88.
40. Ebadi-Dehaghani H, Khonakdar HA, Barikani M, Jafari SH. Experimental and theoretical analyses of mechanical properties of PP/PLA/clay nanocomposites. Compos- Part B. 2015;69:133–44.